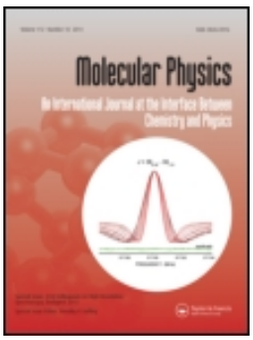

Taylor & Francis
Taylor & Francis Group

Molecular Physics

An International Journal at the Interface Between Chemistry and Physics

ISSN: 0026-8976 (Print) 1362-3028 (Online) Journal homepage: http://www.tandfonline.com/loi/tmph20

From quantum chemistry to dissociation kinetics: what we need to know

Jürgen Troe

To cite this article: Jürgen Troe (2014) From quantum chemistry to dissociation kinetics: what we need to know, Molecular Physics, 112:18, 2374-2383, DOI: 10.1080/00268976.2014.927078

To link to this article: http://dx.doi.org/10.1080/00268976.2014.927078

Published online: 23 Jun 2014.

Molecular Physics, 2014
Vol. 112, No. 18, 2374–2383, http://dx.doi.org/10.1080/00268976.2014.927078

INVITED ARTICLE

From quantum chemistry to dissociation kinetics: what we need to know†

Jürgen Troe*

Institut für Physikalische Chemie, Universität Göttingen, and Max-Planck-Institut für Biophysikalische Chemie, Göttingen, Germany

(*Received 25 February 2014; accepted 15 May 2014*)

The relationship between rate constants for dissociation and the reverse association reactions and their potential energy surfaces is illustrated. The reaction systems $e^- + SF_6 \leftrightarrow SF_6^- \rightarrow SF_5^- + F$, $H + CH_3 \leftrightarrow CH_4$, $2\,CF_2 \leftrightarrow C_2F_4$, $H + O_2 \rightarrow HO_2$, $HO + O \leftrightarrow HO_2 \leftrightarrow H + O_2$, and $C + HO \rightarrow CHO$ are chosen as representative examples. The necessity to know precise thermochemical data is emphasised. The interplay between attractive and anisotropic components of the potentials influences the rate constants. Spin–orbit and electronic–rotational coupling in reactions between electronic open-shell radicals so far generally has been neglected, but is shown to have a marked influence on low temperature rate constants.

Keywords: reaction kinetics

1. Introduction

Dissociation and the reverse association reactions play an important role in combustion, atmospheric and interstellar chemistry, as well as in many other gas-phase reaction systems. While the energy levels of the reacting species generally are well known from high-resolution molecular spectroscopy and quantum chemical calculations, the dissociation and association rates are much less precisely measured and rate theories are generally far from being satisfactory. By presenting a few examples, this essay describes the state of the art and highlights areas where priority needs for determining rate parameters can be identified.

Electron attachment to SF_6 and the reverse detachment from SF_6^- in competition to the dissociation of SF_6^- is chosen as the first example. This system is of considerable fundamental and practical importance and it has been studied in detail over some time. Many characteristic features of plasma chemical kinetics are encountered here and progress in the understanding can be documented particularly well. Thermal dissociation of methane is of similar importance in hydrocarbon pyrolysis and oxidation and hence in combustion chemistry. This system has been chosen because theoretical studies of its elementary processes – collisional energy transfer between the excited molecule and its surrounding bath gas as well as intramolecular bond breaking and bond formation – are reaching a mature state without the necessity for empirical adjustment of parameters. The thermal dissociation of perfluoroethene and the reverse dimerisation of difluorocarbene are described for comparison, again illustrating the present understanding, but in addition emphasising the basic differences between hydrocarbon and fluorocarbon dissociation and association kinetics. Finally, the 'simple' reaction system $H + O_2 \leftrightarrow HO_2 \leftrightarrow HO + O$ is analysed with respect to various aspects of dissociation and association dynamics. The open-electronic shell character of the reactants renders a quantitative analysis of the dynamics particularly difficult. The effects to be expected are illustrated by a comparison with the $C + HO$ association process for which the consequences of spin–orbit coupling have already been analysed. The interplay between attractive and anisotropic components of the potential energy surface, as in the CH_4 and C_2F_4 systems, is illustrated also for the HO_2 system with respect to its influence on the dissociation and association dynamics.

In summary, this report describes which properties of potential energy surfaces and which details of the reaction dynamics on these potentials need to be known with priority in order to arrive at least at a semiquantitative understanding of dissociation and the reverse association processes.

2. Kinetics of the $e^- + SF_6 \leftrightarrow SF_6^- \rightarrow SF_5^- + F$ reaction system

The inert, non-toxic, and insulating molecule SF_6 is used in many technical applications. For example in the plasma etching of silicon chips the reaction $SF_6 + e^- \rightarrow SF_5^- + F$ acts as a source for fluorine atoms which may remove unprotected silicon in a reaction $4\,F + Si \rightarrow SiF_4$. By acting as an 'electron sponge', SF_6 efficiently reduces the concentration of mobile electrons from ionised gases. Because of this ability, SF_6 may be used to shape switching arcs in circuit breakers of power plants and here finds wide practical

* Email: shoff@gwdg.de
† The Molecular Physics Lecture presented at the 23rd Colloquium on High Resolution Molecular Spectroscopy, Budapest, August 2013.

applications. While it is a very useful substance, one has to ask whether it is harmless. It is a powerful greenhouse gas, being 20,000 times more effective (per weight) than CO_2 with an atmospheric increase of 4% per year. Its atmospheric lifetime is more than 1000 years; its removal may involve photolysis or the considered reaction $e^- + SF_6 \rightarrow SF_5^- + F$. For the described reasons, the large interest in the kinetics of this reaction system thus is understandable.

The first question to ask obviously is about the thermochemistry of the reaction, in particular about the electron affinity E_a of SF_6, i.e. the energetics (at 0 K) of the reaction $e^- + SF_6 \rightarrow SF_6^-$. Surprisingly, this quantity for a long while could be estimated only by indirect methods [1] giving $E_a = 1.05$ eV, a photoelectron spectrum including the 0–0 transition not being easily accessible. However, the derived value of E_a differed considerably from quantum chemical results. For example CCSD(T)/6-311 + G(2df) calculations led to [2] $E_a = 0.92$ eV. In this situation, a more direct experimental access to E_a was searched and finally found in the measurements of the thermal rate constants for electron attachment $e^- + SF_6 \rightarrow SF_6^-$ and the reverse electron detachment [3]. Although only a small temperature range could be covered for detachment (590 to 670 K), the equilibrium constant K_c in this range became accessible. A third law analysis of K_c could be made, using vibrational frequencies from MP2/aug-cc-pvdz calculations. The result of this analysis was a value of $E_a = 1.20$ eV, the discrepancies thus remaining unsolved. Over the last years, the problem finally found a surprising solution. First, CCSD(T) calculations with larger AO basis sets [4] than used before on the one hand confirmed the small value $E_a = 0.94$ eV; on the other hand, a distorted C_{4v} geometry of SF_6^- was found in contrast to earlier conclusions about an O_h geometry. In addition, highly anharmonic unseparable vibrations were obtained. This prompted [5] a revised third law analysis of the experimental K_c, now leading to $E_a = 1.03 \pm 0.05$ eV, which was in agreement with the earlier less direct determinations, but still far off the much lower quantum-chemical value. The solution of the dilemma finally was reached by new quantum-chemical calculations including a series of higher order (such as scalar-relativistic, inner-shell, and post-CCSD(T), and other) corrections [6]. It was found that, instead of cancelling, these added up, moving the calculated value from $E_a = 0.94$ to 1.0340($\pm$0.03) eV. The described studies, finally leading to quite satisfactory agreement between experiment and theory, illustrate the large effort sometimes required to obtain at least the thermochemical basis for a proper analysis of dissociation/association kinetics. (It should be noted that most recent studies again questioned the agreement [7]. By analysing lifetime distributions of particularly long-lived anions in cooled ion traps, a value of 0.91 eV close to the uncorrected quantum-chemical value of 0.94 eV was derived such that further work is needed again.)

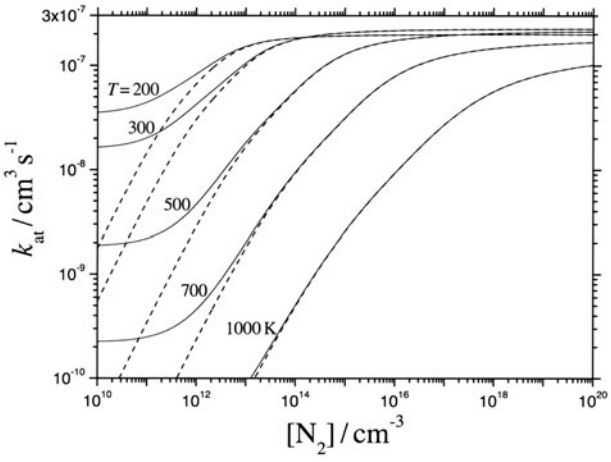

Figure 1. Falloff curves of the rate constants k_{at} for non-dissociative electron attachment to SF_6 (modelling from Ref. [8]; dashed lines: only collisional stabilisation, full lines: collisional plus radiative stabilisation of SF_6^{-*}).

The attachment of electrons by SF_6 takes place in a charge-polarisation potential of r^{-4}-distance dependence. A classical description of the orbital motion of electrons and SF_6 would lead to the Langevin capture rate constant $k_{cap} = 2\pi e\,(\alpha/\mu)^{1/2}$ (e = electronic charge, $\mu \approx$ electronic mass, α = polarisability of SF_6). However, the motion of the electron is not classical. Instead, s-wave quantum scattering governs the process. In addition, the process is of non-Born–Oppenheimer type with coupling between electron and nuclear motions such that the simple Langevin approach cannot be applied. Unlike the Langevin capture rate constant, k_{cap} now depends both on the gas and the electron temperature, and even on gas pressure (see, e.g. Refs [8,9]). It needs collisions with other molecules in the bath gas to stabilise the vibrationally highly excited SF_6^{-*}. Alternatively, the stabilisation may be radiative, i.e. may involve IR emission. Figure 1 shows modelled pressure dependences of thermal attachment rate constants $k_{at}(T, P)$. If stabilisation does not take place, SF_6^{-*} either autodetaches the electron or fragments to $SF_5^- + F$. The latter process again is governed by a charge-polarisation potential (at least at long range). Statistical rate theory allows one to model the energy E- and angular momentum J-specific rate constants for electron detachment and ion fragmentation [10]. Figure 2 shows a comparison for $J = 0$. At low energies, autodetachment dominates, whereas dissociation takes over at energies above the dissociation energy. Obviously, the onset of the two processes is also determined by the value of the electron affinity of SF_6 given above.

The cross sections for dissociative electron attachment [11, 12] to SF_6 have a peculiar shape such as illustrated in Figure 3. At low energies, the decrease reflects the decrease of the capture cross section with increasing electron energy E_{el}. Here, the temperature-dependent high energy tail of the

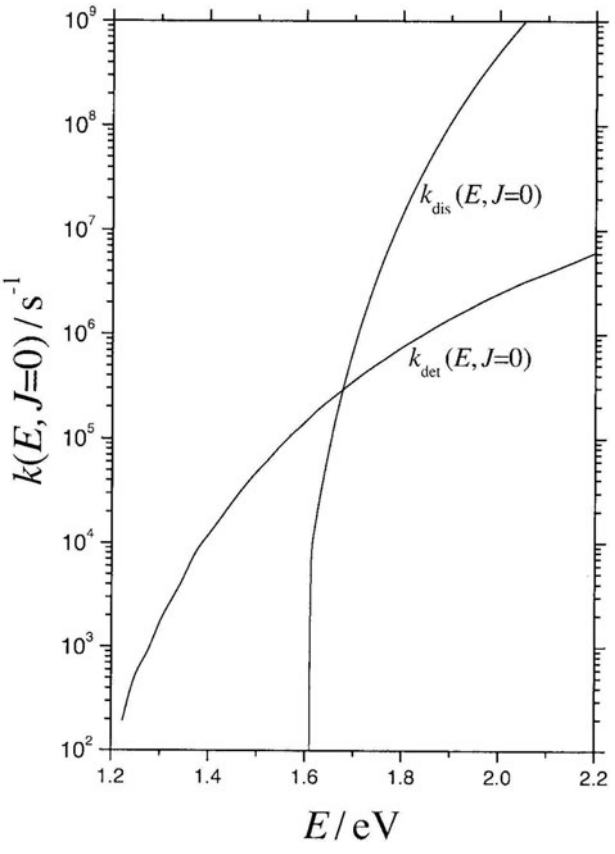

Figure 2. Specific rate constants for electron detachment (k_{det}, $SF_6^- \rightarrow SF_6 + e^-$) and dissociation ($k_{dis}$, $SF_6^- \rightarrow SF_5^- + F$) of SF_6^{-*} (modelling from Ref. [10]; the energies E should be decreased by 0.17 eV after re-evaluation [6] of E_a).

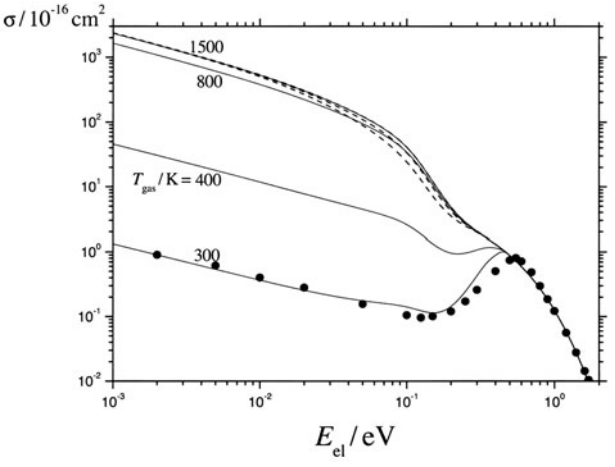

Figure 3. Dissociative electron attachment cross sections of SF_6 as a function of electron energy E_{el} and gas temperature T_{gas} (experimental points from Ref. [11]; modelling from Ref. [10], dashed curves: total cross sections).

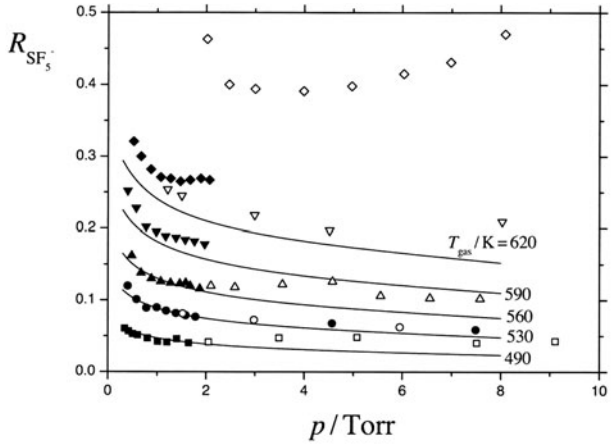

Figure 4. Branching fractions $R = [SF_5^-] / ([SF_6^-] + [SF_5^-])$ for dissociative electron attachment to SF_6 (filled experimental points after 4 ms of reaction time, open experimental points after 14 ms, from Ref. [4]; low-pressure decrease of R: collisional stabilisation of primary SF_6^{-*}, high-pressure increase of R: collisional thermal dissociation of SF_6^- after primary collisional stabilisation of primary SF_6^{-*}).

Boltzmann distribution of thermal SF_6 molecules (together with the electron energy) produces some SF_6^{-*} which is capable of dissociation. With increasing electron energy, E_{el} finally exceeds the dissociation energy of SF_6^{-*}. Then the sum of E_{el} and the thermal energy of SF_6 leads to increasing ion fragmentation, before finally the drop of the capture cross section leads to the marked decrease of the dissociative cross section at large E_{el}. What looks like a 'resonance in the cross section' near $E_{el} = 500$ meV has nothing to do with a resonance, but is the result of a competition of several rate processes and their convolution over energy distributions.

Similar to the dissociative cross sections, also the product branching fractions $R = [SF_5^-]/ ([SF_5^-] + [SF_6^-])$ have a peculiar shape such as shown in Figure 4. The decline of R at lower pressures in Figure 4 corresponds to collisional quenching of the excited SF_6^{-*} produced by the primary electron attachment, while the increase of R at higher pressures (for $T = 620$ K) is brought about by the thermal reactivation of SF_6^- after primary collisional quenching. Kinetic modelling allows one to understand the details of the shown $R(T, P)$ (see Ref. [3]).

From quantum chemistry to dissociation kinetics: what we need to know in this case, first, obviously is the proper thermochemistry. Then, the non-Born–Oppenheimer electron attachment (and detachment) dynamics needs to be understood which is far from being the case today. Instead, empirical models still are necessary to bridge unknown territory (see Ref. [10]). Finally, the dissociation dynamics and collisional deactivation of highly excited molecular ions needs to be quantified. The latter has much in common with the analogous processes for neutral molecules

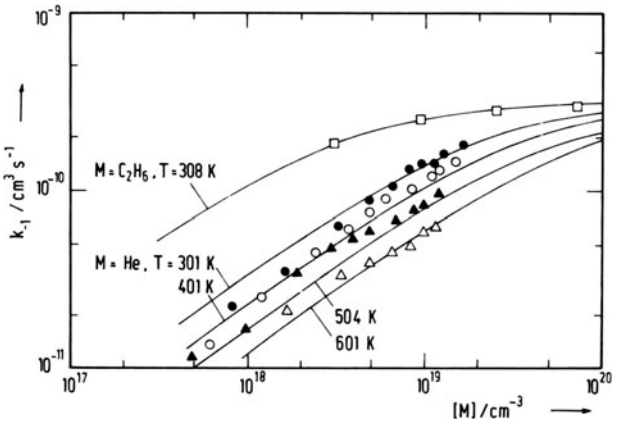

Figure 5. Falloff curves for H + CH_3 (+ M) → CH_4 (+ M) (full lines: modelling from Ref. [13], experimental data given in Ref. [13]).

although the potential energy surfaces and the properties of collisional energy transfer are different. Nevertheless, such processes for ionic and neutral species should be treated on a common level. The following sections present examples for neutral reaction systems.

3. Dissociation/recombination studies in the $CH_4 \leftrightarrow CH_3 + H$ and $C_2F_4 \leftrightarrow 2\,CF_2$ reaction systems

The temperature and pressure dependence of methane dissociation CH_4 (+ M) → CH_3 + H (+ M) and the reverse combination of CH_3 with H to form CH_4 have been investigated in remarkable detail and are particularly suitable for a demonstration of the present situation. Examples [13, 14] of experimental pressure dependences (or dependences on the bath gas concentrations [M]) at fixed temperatures are shown in Figures 5–7. The so-called 'falloff curves', log k vs. log [M], reach from low-pressure ($k \propto$ [M]) to high-pressure behaviour (k independent of [M]). Figures 5–7 illustrate experimental data and modelling results (full curves). The high-pressure limiting behaviour corresponds to a capture of H by CH_3 (for combination) on the potential energy surface of CH_4 (see Refs [15–17] and, for more details, see [18–20]). The low-pressure behaviour reflects the properties of collisional energy transfer on CH_4–M potential energy surfaces (see Refs [21,22]). As the two potentials now are known, one may perform a complete modelling of the reaction dynamics on these surfaces and study how close the experiment and theory come. At the same time, one may ask which details of the potentials matter most and which would be the minimum knowledge required for a meaningful comparison of experiment and theory.

We first consider the high-pressure limit of the CH_4 reaction system governed by the CH_4 potential only. Two properties of the potential turn out to be of primary importance: the minimum-energy path (MEP) potential and the anisotropy of the potential. In the CH_4 case, a Morse-type MEP potential fairly well reproduces the *ab initio* results (see Ref. [20]). Using the MEP potential only and treating the orbital motion of H around CH_3 leads to a capture rate constant (analogous to the Langevin rate constant in electron capture, see above) such as described by phase-space theory (PST) or loose activated complex theory. However, the presence of an anisotropy of the potential reduces the capture rate by introducing 'dynamical hindrance' (or 'tightening of the activated complexes'). One way to account for this effect is the use of a model potential. For example, a potential of the form

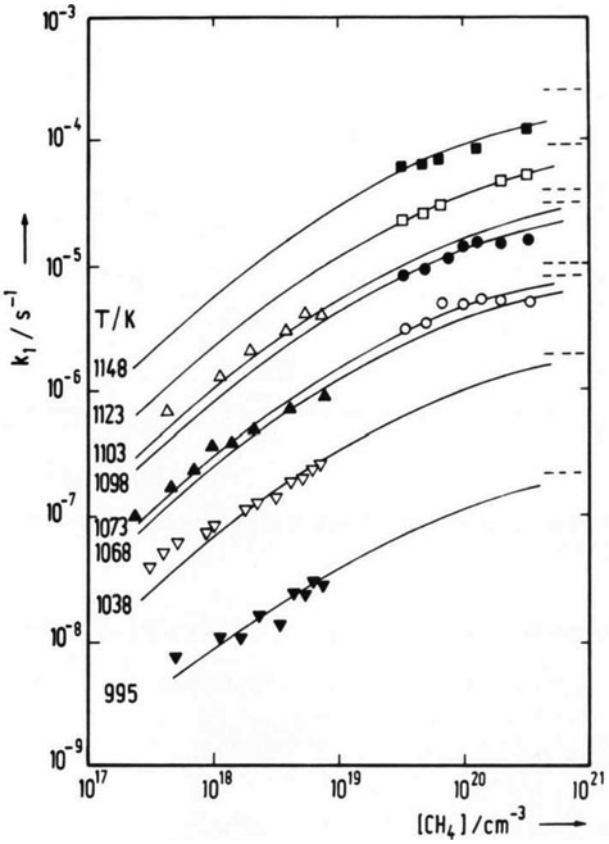

Figure 6. Falloff curves for CH_4 (+ M) → CH_3 + H (+ M) (M = CH_4, modelling from Ref. [13], experimental data given in Ref. [13]).

$$V(r,\theta) = D\{\exp[-2\beta(r-r_e)] - 2\exp[-\beta(r-r_e)]\} + C\exp[-\beta(r-r_e)]\sin^2(\theta-\pi/2) \qquad (3.1)$$

was considered in Ref. [14] (with a fitted Morse parameter β, the dissociation energy D, the H–CH_3 distance r, the angle θ between the H–CH_3 line and the CH_3 plane, and an anisotropy amplitude factor C). Alternatively [23], one may employ a different decay parameter α in the second

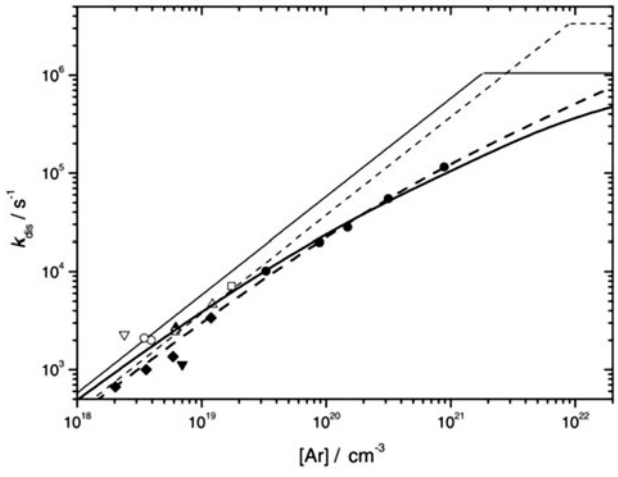

Figure 7. Falloff curves for CH_4 (+ M) → CH_3 + H (+ M) (M = Ar, $T = 2200$ K; full and dashed lines: modelling from Ref. [14], experimental data given in Ref. [14]).

term of Equation (3.1), e.g. here replace β by 2α and determine C from the corresponding deformation vibrations at $r = r_e$. *Ab initio* potentials obviously differ from this simple form. Therefore, two possibilities to characterise an average overall anisotropy have been tested. First, the high-pressure capture rate constant was calculated by classical trajectories both on the *ab initio* potential and on the model potential, which allowed for a fit of the ratio C/D (as done in Ref. [14]). Second, transitional-mode frequencies along the MEP of the *ab initio* potential were determined and trajectory calculations were performed on the corresponding model potential (such as described for the reaction $2CF_2 \rightarrow C_2F_4$ below). Figure 8 illustrates the results for the CH_4 system. The upper points are for the isotropic potential, i.e. for

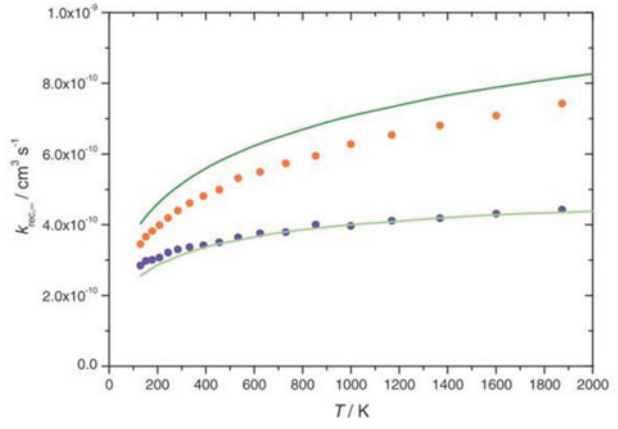

Figure 8. High-pressure limiting rate constants for $CH_4 \rightarrow CH_3$ + H (theoretical modelling from Ref. [14]; lines: modelling with potential of Equation (3.1) and $C/D = 2.5$, points: modelling with the *ab initio* potential of Refs [16, 17]; upper line and points: isotropic potential, i.e. PST, lower line, and points: anisotropic potential).

PST, either from the Morse model potential or from the *ab initio* potential, the lower results are for the full anisotropic potential (points from the *ab initio* results and the line with the model potential of Equation (3.1) and a fitted ratio $C/D = 2.5$). One observes that the simple model potential works as well as the complete *ab initio* potential, confirming that the MEP potential and an average overall anisotropy parameters need to be known with first priority, while further details of the potential are less important for kinetic quantities like dissociation/association rates. The reduction of the capture rate constant by the anisotropy of the potential is well illustrated in Figure 8, PST overestimating the rate by about a factor of 2. We note that the analysis of the *ab initio* potential of Ref. [16] in Ref. [14] led to an effective Morse parameter $\beta \approx 2$ Å^{-1}, while the analysis of the anisotropy of the *ab initio* potential in Ref. [19] gave $\alpha \approx 0.7$–0.8 Å^{-1} (being close to the value of 1 Å^{-1} suggested long ago in Ref. [23]). With a ratio $\alpha/\beta \approx 0.4$ this close to the 'normal' ratio of 0.5 derived from a series of typical dissociation and recombination reactions in Ref. [24].

The low-pressure limiting rate constant requires solution of the master equation for intermolecular collisional energy transfer [21,22,25–27]. Assuming very efficient energy exchange, 'strong collision rate constants' are obtained as upper limits, only containing an overall collision number. The assumption that the latter can be identified with the Lennard-Jones collision number has been confirmed by classical trajectory calculations (see, e.g. Refs [21,22] for CH_4 collisions with inert colliders M). On the other hand, more efficient colliders like M = H_2O, are characterised by larger collision numbers Z (see, e.g. Refs [22,28]). When collisional energy is less efficient, the rate constant is reduced by a 'collision efficiency' β_c, being related to the average energy transferred per collision $<\Delta E>$. The contribution of vibrational and rotational energy transfer to $<\Delta E>$ has been investigated in detail [21,25]. Again minor details do not matter too much, but an almost temperature independent $<\Delta E>$ in practice generally has to be used as a fit parameter (a temperature independence of $<\Delta E>$ corresponds to [25] an increase of the average energy transferred per down collision $<\Delta E_{down}> \propto T^{1/2}$). The necessity to use this fit parameter obviously presents a limitation to the prediction of low-pressure rate constants. For the methane system, this problem has been overcome. Here, the trajectory calculations of Ref. [21] on the *ab initio* potential for the CH_4–M interaction led to $<\Delta E>$ values in agreement with values derived by evaluating experimental low-pressure rate constants [28].

With the information on the dissociation/association and collisional energy transfer dynamics obtained from calculations on *ab initio* potentials and simplified versions of such potentials, one is in the position to model full falloff curves of the dissociation/association reactions [14,26]. The results of such modelling are included in Figures 5–7. Obviously kinetics averages out finer details of the

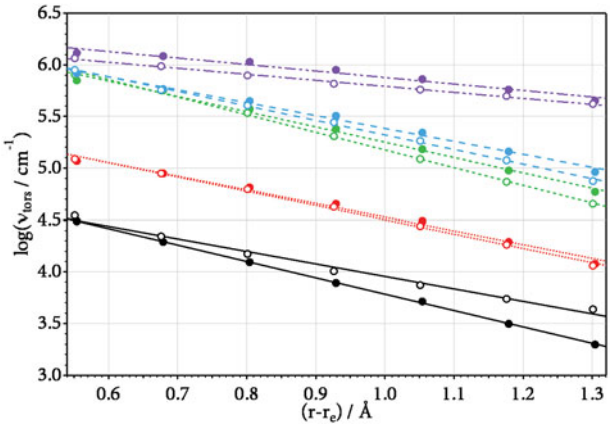

Figure 9. Dependence of transitional mode frequencies on the C–C bond length r in C_2F_4 (quantum-chemical calculations from Ref. [30], $\alpha/\text{Å}^{-1}$ = anisotropy parameter, see the text).

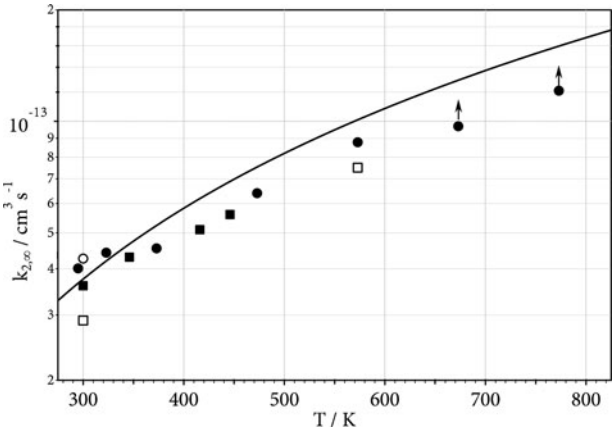

Figure 10. High-pressure limiting rate constants for 2 $CF_2 \rightarrow C_2F_4$ (line: SACM/CT calculations from Ref. [30] with $\alpha/\beta \approx 0.23$, experimental data given in Ref. [30]).

potentials and of the dynamics and only few key properties need to be known. These are the parameters D, β, and C (or α/β) on the side of the intramolecular potential of Equation (3.1), and Z and $<\Delta E>$ on the side of the collisional energy transfer.

The interplay between the attractive and anisotropic parts of the potential in dissociation/association dynamics has been demonstrated extensively with the statistical adiabatic channel model (SACM) [23] in combination with classical trajectory calculations (CT) [29]. In the original version [23] of the SACM, the anisotropy of the potential was expressed by the quantum states of deformation motions, changing from bending vibrations into free rotations along the MEP of dissociation. We illustrate this feature of an anisotropic potential for the $C_2F_4 \rightarrow 2CF_2$ dissociation. Figure 9 shows the results of quantum-chemical calculations [30] of vibrational frequencies of five torsional modes as a function of the C–C bond length r. One observes an exponential decay, confirming suggestions from the original SACM [23] and presenting the mentioned alternative to the anisotropy of the model potential of Equation (3.1). Inserting the corresponding ratio of the decay parameter $\alpha \approx 1.2$ Å^{-1} and the effective Morse parameter $\beta \approx 5.2$ Å^{-1}, i.e. $\alpha/\beta \approx 0.23$, into the modelling relationships from SACM/CT calculations [29], leads to high-pressure rate constants which are in close agreement with experimental data [30] (see Figure 10). As the calculation is based on *ab initio* potential data and does not involve additional empirical fit parameters, one concludes that the leading properties of the potential have been characterised realistically and are validated by the experimental results. In particular, the unusually small value of the ratio α/β (being much smaller than the normal value of this ratio such as observed for the CH_4 system described above) is identified to be responsible for the small value of the high-pressure association rate constant and its markedly positive temperature coefficient (see Figure 10).

4. The association reaction H + O_2 ↔ HO_2* followed by HO_2* + M → HO_2 + M

The recombination reaction H + $O_2 \rightarrow HO_2$ plays a key role in the oxidation of hydrogen and hydrocarbons and, thus, is one of the most important reactions of combustion chemistry. Comparing its potential energy surface with that of H + $CH_3 \rightarrow CH_4$, one observes marked differences, mainly in the MEP potential such as illustrated in Figure 11. While the CH_4- and C_2F_4-systems were characterised by simple Morse-type MEP potentials, now there is something like a 'shoulder' in the potential which may be the remnant of an avoided crossing of electronic states. This has profound consequences for the capture dynamics. Employing the *ab initio* potential from Ref. [31], adiabatic channel potential curves were constructed in Ref. [32]. Figure 12 shows examples of such curves, along which the quantum

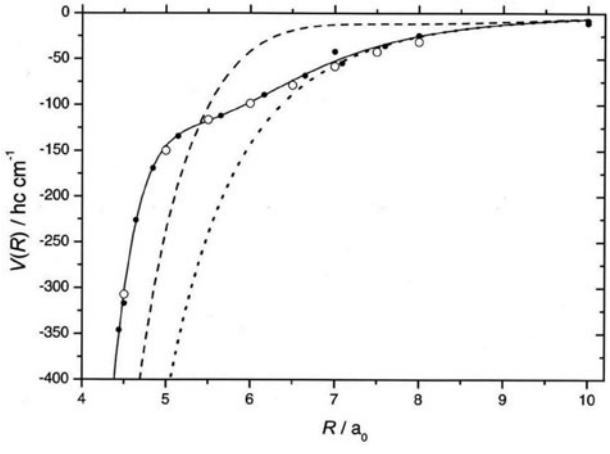

Figure 11. Minimum-energy path potential $V(R)$ for $HO_2 \rightarrow$ H + O_2 ($a_0 = 0.529$ Å, from Ref. [32]; points and full line: *ab initio* potential of Ref. [31], dashed and dotted lines: simpler analytical potentials, see Ref. [32]).

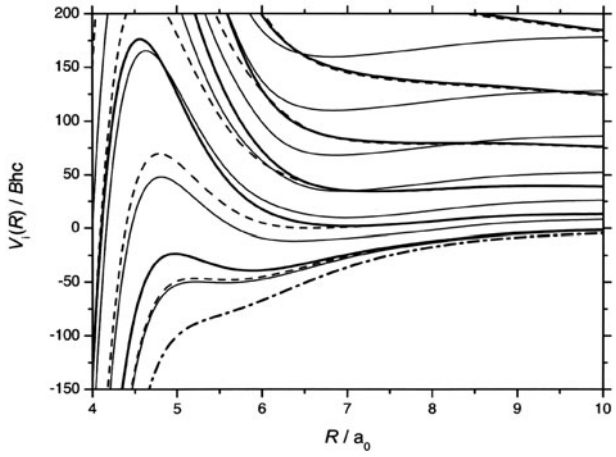

Figure 12. Transition-state switching in the adiabatic channel potential curves $V_l(R)$ for $HO_2 \rightarrow H + O_2$ (SACM calculations from Ref. [32]; $B = 1.446\ cm^{-1}$, dash–dotted line: MEP potential of Figure 11, other lines: channel potentials for $l = j = 1, 3, 5, \ldots$ from bottom to top, see Ref. [32]).

numbers of the HO_2 modes and the quantum number of the $H + O_2$ orbital motion of the dynamics adiabatically are kept constant. One notices 'transition state switching' from large H–O_2 distances for low energy to H–O_2 distances near $4.5a_0$ (= 2.4 Å) for higher energies. The consequences for the capture dynamics are considerable. Figure 13 shows thermal capture rate constants, in the upper curve for PST (neglecting the anisotropy of the potential) with clear evidence for transition state (TS) switching, from an outer TS at low temperatures to an inner TS at temperatures above about 50 K. Taking into account the anisotropy of the potential, the capture rate constant k_{cap} decreases to the lower curve, but still showing the consequences of TS switching.

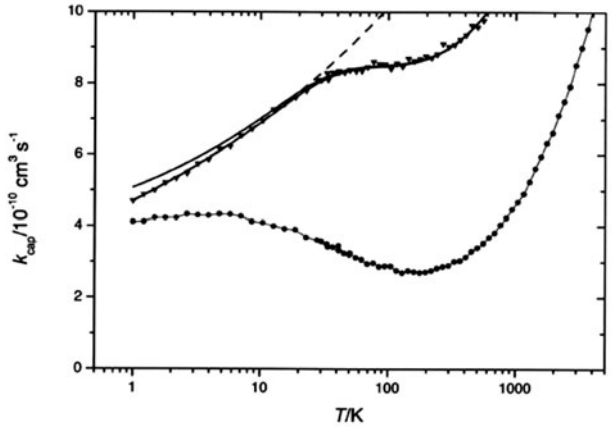

Figure 13. Capture rate constants k_{cap} for $H + O_2 \rightarrow HO_2$ (from Ref. [32], dashed line: with isotropic long-range potential, upper full line: PST with MEP potential of Figure 11, lower full line: with anisotropic *ab initio* potential from Ref. [31]).

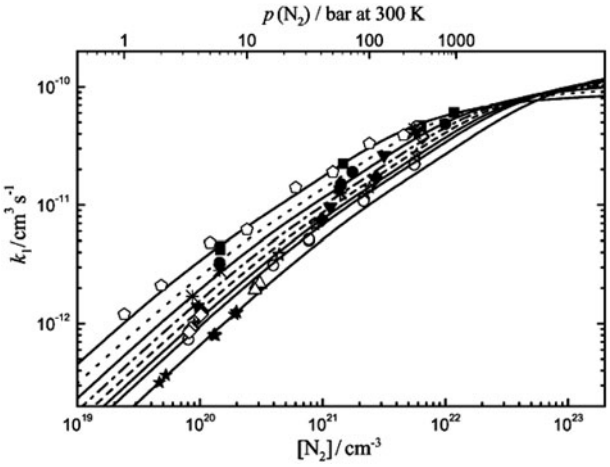

Figure 14. Falloff curves for $H + O_2 + M \rightarrow HO_2 + M$ (from Ref. [28], M = N_2, experimental points given in Ref. [28], T = 300, 400, …, 900, and 1200 K from bottom to top).

In the $H + O_2$ system, we first encounter the 'open-shell dilemma' of radical–radical reactions. All reaction partners are in open-electronic shells: $H(^2S_{1/2})$, $O_2(^3\Sigma_g)$, and $HO_2(^2A'', {}^4A'')$. The question arises which of the fine-structure states contribute to the reaction. Simply assuming that only the lowest states with a thermal population $f_{el}(T)$ are relevant, conventionally one assumes that the high-pressure recombination rate constant $k_{rec,\infty}$ here is given by

$$k_{rec,\infty} \approx f_{el}(T) k_{cap} \qquad (4.1)$$

with $f_{el}(T) = 1/3$ (at 'not too low temperatures' and assuming that only doublets contribute). We come back to this point in the next section. Comparing this calculated $k_{rec,\infty}$ with experimental falloff curves from Ref. [28], one obtains very good agreement (see Figure 14). The agreement even reaches over into the liquid phase, where $H + O_2 \rightarrow HO_2$ plays an important role in the radiation chemistry of water [33]. For the full falloff curves [28], one needs information on collisional energy transfer again such as described above for the $CH_4 + M$ system. One should mention that M = H_2O is a particularly efficient collider. It was suggested in Ref. [28] to identify the corresponding collision number Z with an HO_2–H_2O dipole–dipole capture rate constant instead of a Lennard-Jones collision number.

5. Open-electronic shell effects in radical–radical reactions

The question arises whether Equation (4.1) applies in general, i.e. whether a capture-controlled bimolecular reaction of open-electronic shell radicals proceeds on a single- potential energy surface, connecting the lowest electronic fine-structure states of the reactants with the electronic ground

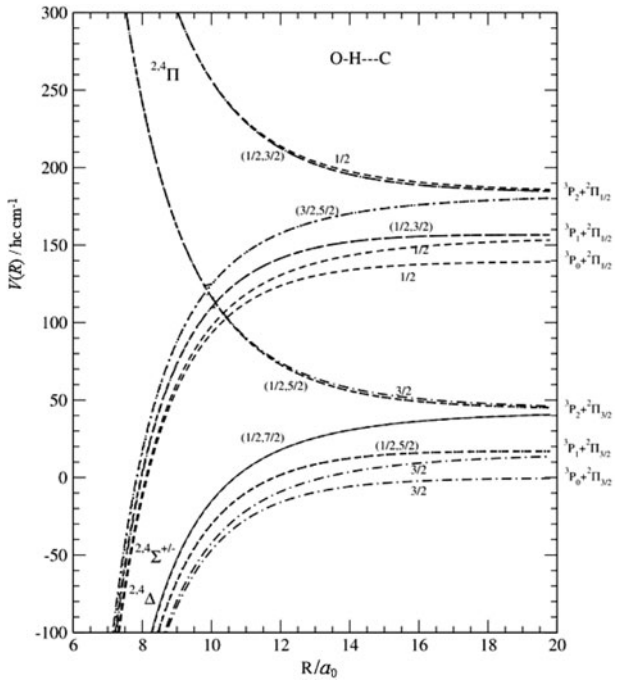

Figure 15. Long-range potential energy curves for C + HO → CHO (from Ref. [34], numbers = Ω values).

state of the intermediate adduct, and whether Equation (4.1) accounts for this. The fine-structure states at large distances generally are degenerate or nearly degenerate. When the reactants approach each other, then there may be a multitude of electronic states of the adduct, before the latter states sufficiently separate at close approach. Figure 15 illustrates such a situation [34] for the association process C + HO → CHO. During the capture kinetics, there will be efficient non-Born–Oppenheimer mixing of the shown states. In order to quantify this mixing, the potential has to be determined including long-range electrostatic, dispersion, induction, and exchange interactions; in addition spin–orbit and electronic–rotational coupling has to be taken into account. The reaction C + HO → CHO is the single example where the corresponding non-Born–Oppenheimer coupling dynamics has been implemented into an adiabatic channel treatment accounting for electronic–rotational (rotronic) couplings [35]. The results of this generalised SACM treatment using asymptotic potentials here were compared with detailed calculations based on Equation (4.1), see also Ref. [36]. Figure 16 compares the resulting association rate constants k_{ass}. Over the range 15–200 K, the non-Born–Oppenheimer rate constant markedly exceeds the single-potential rate constant based on Equation (4.1) ($k_{rec,\infty}$ and k_{ass} are equivalent). Apparently, rotronic coupling within the multitude of electronic states arising from the degenerate separated reactants generates a large amount of state mixing. This then leads to contributions from higher

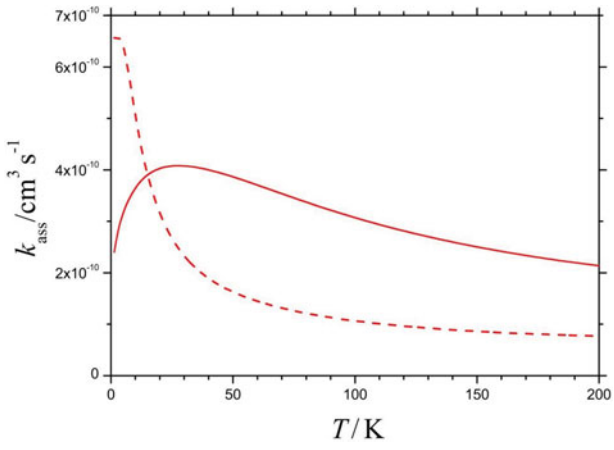

Figure 16. Association rate constants for C + HO → CHO (from Ref. [35]; $k_{ass} = k_{rec,\infty}$, dashed line: calculation with single electronic state and Equation (4.1), full line: calculation with full mixing of electronic states accounting for spin–orbit and rotronic coupling).

fine-structure states to capture into the electronic ground state of the adduct.

Other radical–radical reactions should be treated in a similar way. There is particular interest in the reaction HO + O → HO_2 → H + O_2. Low temperature experimental rate constants are shown in Figure 17. The experimental rate differ considerably below about 150 K. One would hope that theory helps to settle the situation. It looks that full quantum time-independent calculations of cross sections and classical trajectory calculations from Ref. [37] favour the lower experimental values. However, these theoretical results were based on Equation (4.1) and did not account for rotronic couplings like those treated for C + HO in Ref. [35]. Figure 17 may suggest that the latter effects raise the

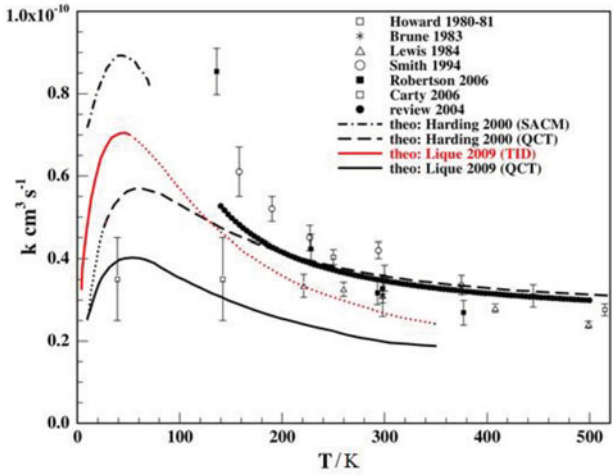

Figure 17. Experimental (points) and modelled (lines) low temperature rate constants for HO + O → H + O_2 (from the Kinetic Database for Astrochemistry (KIDA) [38]).

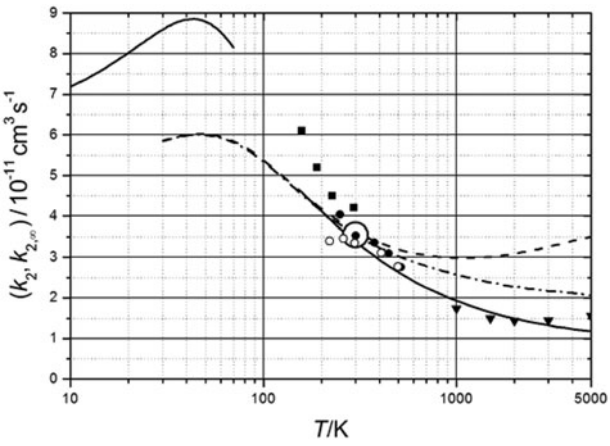

Figure 18. Rate constants for HO + O → H + O_2 (various models from Ref. [40] compared with experimental points, for details see Ref. [40]; high temperature points from the reverse reaction converted with the equilibrium constant).

rate constants to the upper values shown [38]. First steps towards a non-Born–Oppenheimer treatment of the reaction HO + O → HO_2 have been done in Ref. [39], but more work is required. Extending the temperature range of Figure 17 up to 5000 K, where data for the reverse reaction H + O_2 ⇔ HO_2 → HO + O are available, one reaches conditions where a single-potential Born–Oppenheimer treatment becomes sufficient. Figure 18 compares the detailed results from Ref. [40] with experiments. Here, from 300 to 5000 K, experiment and theory agree satisfactorily without that reaction parameters have to be empirically fitted. However, this agreement was only obtained after the enthalpy of formation of the OH radical finally could be established in Ref. [41]. Without proper thermochemistry such agreement could not have been reached.

6. Conclusions

From quantum-chemistry to dissociation dynamics: of course, a complete and accurate knowledge of the potential energy surface(s) of the reaction would be desirable to have and quantum-scattering calculations on the potential(s) should be made. However, this may involve enormous effort whose finer results would finally be lost by thermal averaging. Therefore, the simpler approaches described here may provide sufficient insight for the time being and a combination of the semiquantitative theoretical results with experimental data may lead to the presently most realistic values of the rate constants.

References

[1] E.P. Grimsrud, S. Chowdhury, and P. Kebarle, J. Chem. Phys. **83**, 1059 (1985).
[2] G.L. Gutsev and R.J. Bartlett, Mol. Phys. **94**, 121 (1998).
[3] A.A. Viggiano, T.M. Miller, J.F. Friedman, and J. Troe, J. Chem. Phys. **127**, 244305 (2007).
[4] W. Eisfeld, J. Chem. Phys. **134**, 054303 (2011); **134**, 129903 (2011).
[5] J. Troe, T.M. Miller, and A.A. Viggiano, J. Chem. Phys. **136**, 121102 (2012).
[6] A. Karton and J.M.L. Martin, J. Chem. Phys. **136**, 197101 (2012).
[7] S. Menk, S. Das, K. Blaum, M.W. Froese, M. Lange, M. Mukherjee, R. Repnow, D. Schwalm, R. von Hahn, and A. Wolf, Phys. Tev. A **89**, 022502 (2014).
[8] J. Troe, T.M. Miller, and A.A. Viggiano, J. Chem. Phys. **127**, 244303 (2007).
[9] J. Troe, G. Marowsky, N.S. Shuman, T.M. Miller, and A.A. Viggiano, Z. Phys. Chem. **225**, 1405 (2011).
[10] J. Troe, T.M. Miller, and A.A. Viggiano, J. Chem. Phys. **127**, 244304 (2007).
[11] M.-W. Ruf, M. Braun, S. Marienfeld, I.I. Fabrikant, and H. Hotop, International Conference on Photonic, Electronic and Atomic Collisions Progress Report, Freiburg, July 2007; experimental data included in Ref. [12].
[12] J. Troe, T.M. Miller, and A.A. Viggiano, J. Chem. Phys. **127**, 244304 (2007).
[13] C.J. Cobos and J. Troe, Z. Phys. Chem. **167**, 129 (1990).
[14] J. Troe and V.G. Ushakov, J. Chem. Phys. **136**, 214309 (2012).
[15] M. Lewerenz and M. Quack, J. Chem. Phys. **88**, 5408 (1988).
[16] S.J. Klippenstein, Y. Georgievskii, and L.B. Harding, Proc. Combust. Inst. **29**, 1229 (2002).
[17] L.B. Harding, S.J. Klippenstein, and A.W. Jasper, Phys. Chem. Chem. Phys. **9**, 4055 (2007).
[18] R. Marquardt and M. Quack, J. Chem. Phys. **109**, 10628 (1998).
[19] R. Marquardt and M. Quack, J. Phys. Chem. A **108**, 3166 (2004).
[20] R. Marquardt and M. Quack, in *Handbook of High Resolution Spectroscopy*, edited by M. Quack and F. Merkt (Wiley, New York, 2011).
[21] A.W. Jasper and J.A. Miller, J. Phys. Chem. A **115**, 6438 (2011).
[22] A.W. Jasper, J.A. Miller, and S.J. Klippenstein, J. Phys. Chem. A **117**, 12243 (2013).
[23] M. Quack and J. Troe, Ber. Bunsenges. Phys. Chem. **78**, 240 (1974).
[24] C.J. Cobos and J. Troe, J. Chem. Phys. **83**, 1010 (1985).
[25] J. Troe, J. Chem. Phys. **66**, 4745 (1977).
[26] J. Troe, J. Phys. Chem. **83**, 114 (1979).
[27] T. Baer and W.L. Hase, *Unimolecular Reaction Dynamics. Theory and Experiments* (Oxford University Press, New York, 1996).
[28] R.X. Fernandes, K. Luther, J. Troe, and V.G. Ushakov, Phys. Chem. Chem. Phys. **10**, 4213 (2008).
[29] A.I. Maergoiz, E.E. Nikitin, J. Troe, and V.G. Ushakov, J. Chem. Phys. **108**, 9987 (1998).
[30] C.J. Cobos, A.E. Croce, K. Luther, L. Sölter, E. Tellbach, and J. Troe, J. Phys. Chem. A **117**, 11420 (2013).
[31] L.B. Harding, J. Troe, and V.G. Ushakov, Phys. Chem. Chem. Phys. **2**, 631 (2000).
[32] J. Troe and V.G. Ushakov, J. Chem. Phys. **128**, 204307 (2008).
[33] I. Janik, D.M. Bartels, T. Marin, and C. Jonah, J. Phys. Chem. A **111**, 79 (2007).

[34] B. Bussery-Honvault, F. Dayou, and A. Zanchet, J. Chem. Phys. **129**, 234302 (2008).
[35] A.I. Maergoiz, E.E. Nikitin, and J. Troe, J. Chem. Phys. (2014, to be published).
[36] A. Zanchet, P. Halvick, J.-C. Rayez, B. Bussery-Honvault, and P. Honvault, J. Chem. Phys. **126**, 184308 (2007).
[37] F. Lique, M. Jorfi, P. Honvault, P. Halvick, S.Y. Lin, H. Guo, D.Q. Xie, P.J. Dagdigian, J. Klos, and M.H. Alexander, J. Chem. Phys. **131**, 22104 (2009).
[38] J.C. Loison, P. Honvault, J. Troe, and I. Sims, Kinetic Database for Astrochemistry. <http://kida.obs.u-bordeaux1.fr/datasheets 1502>
[39] A.I. Maergoiz, E.E. Nikitin, and J. Troe, in *Theory of Chemical Reaction Dynamics*, edited by A. Lagana and G. Lendvay (Kluwer Academic Publishers, New York, 2004).
[40] J. Troe and V.G. Ushakov, J. Chem. Phys. **115**, 3621 (2001).
[41] B. Ruscic, D. Feller, D.A. Dixon, K.A. Peterson, L.B. Harding, R.L. Asher, and A.F. Wagner, J. Phys. Chem. A **105**, 1 (2001).